RSC Advances

ROYAL SOCIETY OF CHEMISTRY

www.rsc.org/advances

Journal Name

RSCPublishing

ARTICLE

Pyrite nanotube array films as an efficient photocatalyst for degradation of Methylene Blue and Phenol

Cite this: DOI: 10.1039/xoxxoooooox

Received ooth January 2012,
Accepted ooth January 2012

DOI: 10.1039/xoxxoooooox

www.rsc.org/

Ang Tian,[a,•*] Quan Xu,[b,•] Xiaoguo Shi,[a] He Yang,[a] Xiangxin Xue,[a,*], Junhua You[c], Xiaoqiang Wang,[d,] Chenbo Dong[e] , Xin Yan[b], Hongjun Zhou[b]

Pyrite crystal is used as potential catalyst for the degradation of pollutants or removing waste gas in environmental engineering. However, the traditional pyrite synthetic process could lead to intermediate phases during formation of pyrite, such as FeS or $Fe_{1-x}S$, hurting purity of products. In this study, the pure FeS_2 nanotubes with stoichiometric ratio were fabricated by vulcanizing the precursor nanotubes. The photocatalytic activity of nanotubes was investigated via decomposing the Methylene Blue and phenol. The results indicated that the oxidation of pyrite affected the photocatalytic activity of pyrite nanotubes slightly. Comparing with the pyrite piled microparticles coating and the hematite nanotube coating, the visible light driven catalytic activity of pyrite nanotubes coating was derived from increased production of hydroxyl radicals. The topography of nanotube array contributed to generation of the photoinduced $hole^+$ and separation of the $e^-/hole^+$ pairs, eventually enhanced photocatalysis performance. In addition, Fe_2O_3 nanotubes can decompose MB effectively, however, hardly degrade phenol. This work offers insight to develop transition metal based semiconductor photocatalysts for environmental and energy utilization.

1. Introduction

In order to response to energy crisis and environmental issues in the modern society, it is under urgent to develop novel, user controlled functional materials to solve these problems.[1-3] Among various functional materials, semiconductor photocatalytic materials having ability to utilize the solar energy to degrade the organic pollutants attract worldwide intensive attention due to their specific advantage on the light harvesting and energy conversion,[4,5] including Fe_2O_3 [6], TiO_2 [7], MnO_2 [8] and etc. Specially, TiO_2 has been widely used as the photocatalyst in decades with low cost and easier fabrication for various applications such as solar hydrogen production,[9] decomposing the organic pollutants in solutions[10] or mineralizing the hazardous gas.[11] However, the wide band gap of TiO_2 confined the photo response to the UV spectrum, which occupied only 3-5% of the total energy could be received from the visible light, resulting in low solar energy utilization efficiency. Thus, in order to minimize the band gap to achieve higher solar energy utilization efficiency, different methods include surface modification and element doping on these materials have been performed.[12,13] In addition, the separation of photo-induced electron-hole pair would also regulate the photocatalytic process, attracting increased attention from scholars all over the world. In previous studies, mophology modulating[14] and creation of heterojunction were applied to inhibit the recombination of electron and hole.[15,16] Meanwhile, other considerable semiconductors for sustainable photo catalysis process were developed. Specially, the iron pyrite (FeS_2) has attracted great interest for their high optical absorption ($a>10^{-5}$ cm^{-1}) under the visible electromagnetic spectrum, nontoxicity, environmental compatibility and high quantum efficiency (>80%) characteristics.[17,18]

Many studies have demonstrated that the pyrite could generate the photoelectron under the activation of visible light, especially the pyrite film was the potential candidate of the absorber [17,19,20] and counter electrode in the solar cells [21] for the photovoltaic application. However, the pyrite is p-type near the surface and the high-density surface states would result in the Fermi level pinning, which would trap the photoinduced electrons.[22] In addition, the presence of the iron pyrite phase impurities would also impair the motility of the carrier and small the open circuit voltages.[20,23] Removing the defect states and transferring the low mobility photoinduced carriers could be potential to contribute to the photovoltage,[22] the efforts to improve the photoconductive properties have been undertaken in terms of the synthesis of pure and high crystalline cubic FeS_2 [20,24], supercritical CO_2 co-doping [25] and the size modulating

[19,26]. On the other hand, the photoinduced holes of pyrite could contribute to the photodecomposition of organic pollutants.[27] However, it is regrettable that instead of the photocatalyst, the pyrite has been widely used as the donor of the ferric ion in the pyrite-Fenton catalyst system for the treatment of pollutants, either in gas [28] or aqueous phase [29]. And the mineralization effects caused by the photoinduced hydroxyl radical always performed subordinate role in the catalyst process, which was dependent mainly on the Fenton reaction.[30] To explore pyrite crystal photocatalytic ability, effective modification method is needed to regulate their surface chemical/physical properties.

Topography effects on the semiconductor crystals have been employed to improve the performance on the photocatalyst. [11,31] Specially, the nanotube array structures could significantly enhance the photo harvesting and accelerate the mobility of the photoinduced electrons, which have been demonstrated on the photo electrochemical behaviours of TiO_2 nanotube array films. [15] Additionally, the investigation on the photocatalysis of pyrite films have suggested that the shape and size regulation could lead to the enhanced optical and photoelectric properties.[32,33,34] Previously, our group has shown that high pure crystal FeS_2 nanotube array coatings could be fabricated by vulcanizing precursor nanotubes without formation of marcasite phase, which exhibited excellent optical property and great potential as photocatalyst.[35] Herein we report for the first time on the photocatalytic behaviour of FeS_2 nanotubes coating in degradation of methylene blue (MB) and phenol, the effect of oxidation of pyrite on the photocatalytic process was also investigated.

2. Experiment

2.1 Materials and Fabrication

The nanotube films and the microparticles films were fabricated as previous report described.[35] Prior to anodization, all iron foils (99.9%, 10*10*0.6mm) were polished by sandpaper and degreased ultrasonically in alkali liquor, acetone, ethanol, and distilled water consecutively, followed by drying in nitrogen. Initially, the precursor nanotubes were fabricated by anodization in an ethanediol electrolyte containing 9 wt% NH_4F and 2.7 wt% distilled water under a constant DC voltage of 70 V at 10°C. After anodization, the samples were properly rinsed with distilled water to remove the remaining ions and dried in a nitrogen oven. Then, the nanotube films were sealed in the quartz tube with sulfur. Nitrogen was filled and evacuated into quartz tube for 5 times to ensure the residual gas pressure was less than 1×10^{-2} Pa. FeS_2 nanotubes were generated by vulcanizing the precursor at 400°C for 5h with the rate of 5°C/min. In addition, the FeS_2 microparticles films and hematite nanotube films were fabricated by vulcanizing at 600°C for 10h and annealed at 400°C for 5h in air with the precursor nnaotubes.

2.2 Characterization

The morphology of FeS_2 nanotube coatings was observed using field emission scanning electron microscope (FESEM, ZEISS ULTRA). The crystalline structure of pyrite films was analyzed by X-ray diffraction (XRD, D8211, Huber, Netherlands) with Cu Kα radiation source. The chemical characteristics of films were characterized by X-ray photoelectron spectroscopy (XPS, ESCALAB250, Thermo VG) and Raman spectra (HR800, Raman spectrometer, Horiba Jobin Yvon). The diffraction spot of single FeS_2 nanotube was characterized by the transmission electron microscopy (TEM, JEM-2100). To explore the effect of the surface area on the adsorption of dye, immersion experiment and the FAAS (flame atomic absorption spectrophotometer, Z-2300, Hitachi, Japan) was used to measure the surface area of different samples. 50ml KCl solution with concentration of 2g/L was employed for the immersion test, pyrite nanotube coatings, pyrite microparticles coatings and Fe_2O_3 nanotube coatings were placed into the solutions for 1.5h, respectively. Then the residue of K ions in the solution was detected by the FAAS.

2.3 Photocatalytic degradation of MB and Phenol

Initially, the MB solution with concentration of 5mg/L was prepared. The self-degradation rate of methylene blue under the visible light was recorded with UV spectrophotometer every 50min. The high-pressure xenon lamp (PLS-SEX300UV, Beijing Trusttech Co. Ltd, 300W) with UV-cut optical filter (>420nm, Beijing Trusttech Co. Ltd) was used as visible light (>420nm) source. In this study, FeS_2 microparticle films and Fe_2O_3 nanotube films were set as control group. Before the photocatalysis degradation of MB, the light block experiment was used to investigate the surface absorption property of different films (pyrite nanotubes, hematite nanotubes and pyrite microparticles) on MB. Three different coatings with area of 1 cm×1cm were placed in 50mL dye solution, respectively. The MB solution with sample immersion was stirred for 1.5h in the dark and the concentration change was measured by the UV spectrophotometer. The measurement was conducted every 10min during the period.

The degradation of MB was implemented after the adsorption reached to the equilibrium. The system was irradiated by the fluorescent lamp with stirring. The concentration change of dye solution after irradiation was measured by UV spectrophotometer every 20min. The whole experiment was maintained at ambient temperature

High performance Liquid Chromatography (HPLC) with a C18 reverse-phase column (1260 Infinity, Agilent Technologies, America) was employed to investigate the photocatalytic activity of three different samples via degrading phenol under the visible light illumination. In a typical experiment, taking the pyrite nanotubes for instance, the catalyst was immersed in the 100mL phenol aqueous solution, the concentration of phenol was 15mg/L. The equipment for the photocatalysis has been mentioned above. Respecting to the adsorption equilibrium, before the illumination the solution was stirred under the dark condition for 2h. Then, the solution was

exposed to visible light with stirring for 2.5h. For measuring the degradation rate of phenol, the UV detector in the HPLC was used at a wavelength of 280nm. The mobile phase was the mixed solution of methanol and distilled water (v: v = 0.55:0.45), and the flow rate was 0.3ml/min. For detecting the hydroxyl radicals, the para-chlorobenzoic acid (pCBA) was used to investigate the production of ·OH in the photocatalytic process. 50ml solution with catalyst and 10 μM pCBA were irradiated under the visible light for 2h, and the production of ·OH was measured by the reduction of the pCBA via the HPLC with the UV detector at a wavelength of 232nm, the mobile phase was a solvent mixture of 50% water and 50% acetonitrile, the flow rate was 0.4 ml/min.

In addition, the pH value in the degradation process was detected using the pH meter (Shanghai Leici, PHS-3C) and the Fe element dissolved in the solution were also detected using the flame atomic absorption spectrophotometer (Z-2300, Hitachi, Japan). The SO_4^{2-} concentration was measured by the typical chemical precipitation method.

3. Results and Discussion

3.1 Characterizations of the nanotubes and microparticles coatings

In the fabrication process, the precursor nanotubes were firstly formed by the anodic oxidation method, and then vulcanized in the vacuum conditions or annealed in the air to form FeS_2 nanotubes and Fe_2O_3 nanotubes, respectively. The independent Fe_2O_3 nanotube structured could be observed in Figure 1a. Specially, the diameters and wall thickness of products were 100±10 nm, 10±2 nm, respectively. The peaks of hematite illustrated in XRD pattern in Figure 1d confirmed the coatings after annealed were purely hematite without other ferrous oxidation. By modifying the parameters of the vulcanization, the FeS_2 nanotubes and microparticles films were achieved as Figure 1b and 1c. The increased thickness and roughness of pyrite tube walls could be attributed to the crystal growth in the vulcanization [36], and the thickness and calibres were 15±3nm and 90±10nm, respectively. The curve in the XRD (Fig 1d) pattern excluded the other impurity phase in the pyrite nanotubes, in contrast, the peaks of the FeS and $Fe_{1-x}S$ phases were observed in the curve of FeS_2 microparticles. The appearance of Fe peaks could be attributed to the Fe substrate underneath the nanotubes layer. The cross section morphologies of the nanotubes and microparticles coatings showed the similar thickness with 1.8-2μm.

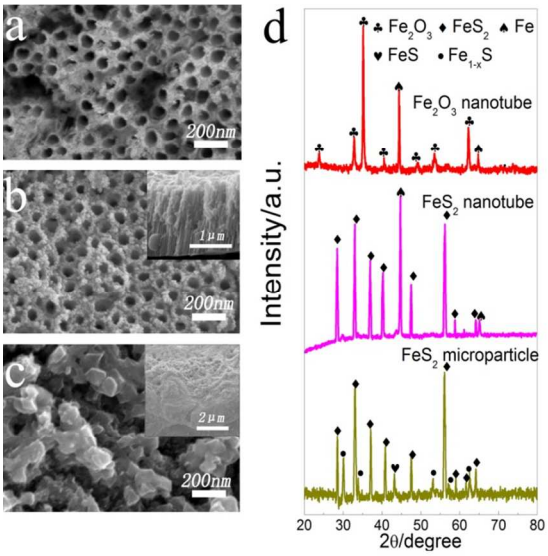

Fig. 1 (a): Morphology of the Fe_2O_3 nanotube array film, (b): morphology of the FeS_2 nanotube array film, (c): morphology of FeS_2 microparticles film, (d): XRD patterns of different films

To further investigate structure and chemical composition of these nanotubes, series characterization technologies include TEM, Raman spectrum and XPS were employed. In the TEM image, the diffraction spots' lattice with spacing of 0.193 nm and 0.309nm associate with the d value of (220) and (111) crystal planes of FeS_2 (pyrite), respectively (Figure 2a). The Raman spectrum was applied to study the chemical bonds and investigate the existence of impurity such as $Fe_{1-x}S$ and marcasite. As shown in Figure 2b, the peaks at 340 cm^{-1} and 377 cm^{-1} were the typical active modes which were caused by the S_2 libration (*E*g) and in phase stretching vibration of S–S dimer (*A*g) in pyrite crystal, respectively.[26] The appearance of peak at 499 cm^{-1} might be attributed to the coupled libration and stretching vibrations or their combination.[37,38] Wide scan XPS spectrum was also employed to investigate the chemical compositions of the nanotube coatings (Figure 2c-e). Four elements Fe, O, C, S were detected in the XPS spectrum. The signal peak of Cls should be derived from the CO_2 in the air, which is usually used for the energy correction of the XPS. In high resolution spectrum (Figure 2d and 2e), the peaks at 707.4eV and 162.2eV were assigned to the typical binding energy of $Fe2p_{3/2}$ and $S2p_{3/2}$ in pyrite crystal [39], and the spin-orbit splitting with 12.9 eV between $Fe2p_{1/2}$ and Fe2p3/2 was consistent with the other study.[40] The peak at 169.0eV is corresponding to ferric sulfates, which was caused by the partly oxidation in the air.[36,41]

3.2 Optical properties

To investigate optical properties of different films, the absorption measurements were performed. The absorption curve in Figure 3 suggested that the absorption coefficient of Fe_2O_3 nanotubes was $1.5\times10^5 cm^{-1}$, the coefficients of pyrite nanotubes and microparticles were $4.2\times10^5 cm^{-1}$ and

$1.75\times10^5 cm^{-1}$, respectively. As the curves showed, all the samples possessed the typical semiconductor characteristics and could absorb visible light. The adsorption of hematite was caused by the direct charge transition in UV region and indirect charge transition in visible region.[42] On the other hand, the optical absorptions of pyrite nanotubes as well as microparticles come from the indirect transition of electron assisting phonons. Specially compared with the FeS_2 microparticle films, the increased absorption coefficient of pyrite nanotubes coatings could be attributed to the nanotube topography which could complete the sulfidation and capture more photons inside the cavity.[35]

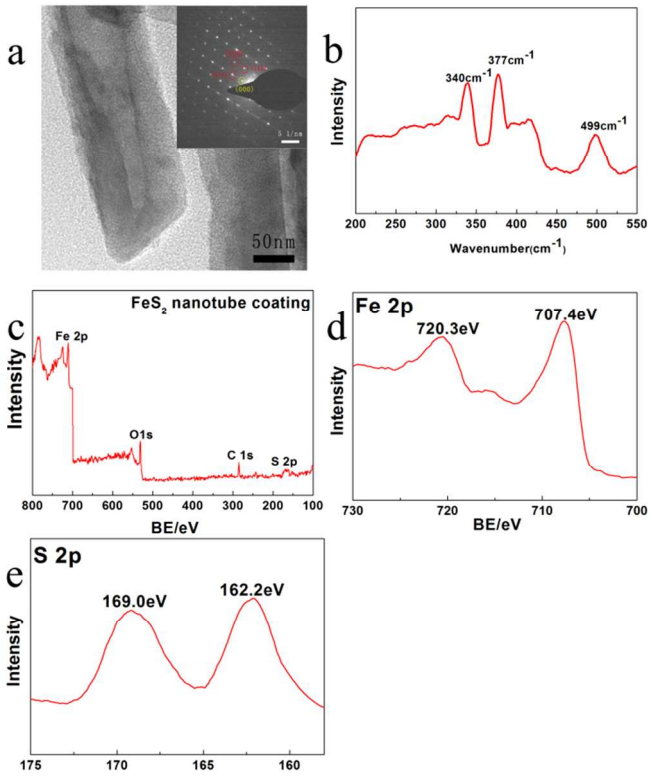

Fig. 2 (a): TEM and diffraction pattern of FeS_2 nanotube, (b): Raman curve of the FeS_2 nanotube film, (c): XPS spectrum of FeS_2 nanotube film, (d-e): high-resolution spectrum of Fe 2p and S 2p

3.3 Degradation of MB and Phenol

To evaluate the photocatalysis ability of the pyrite nanotubes, the degradation of MB under visible light was analyzed. The photocatalysis degradation curve of MB induced by the pyrite nanotubes were illustrated in Figure 4a. The curves of Fe_2O_3 nanotubes and FeS_2 piled microparticles films were used as control (Figure 4b and 4c). For FeS_2 nanotubes, the degradation rate reached to the equilibrium value at 33% with 80 min immersion. On the other hand, the degradation rate of Fe_2O_3 nanotubes and FeS_2 piled microparticles films reached to 30% and 15% with 80 min immersion, respectively. In this study, in order to investigate the degradation of MB under the visible light, the degrade rate was tested after the degradation rate in dark reaching to the equilibrium with 80 min. Under the visible light illumination, the degradation rate of MB for FeS_2 nanotubes was significantly increased, the value reached to about 75% with 200 min. For the Fe_2O_3 nanotubes and the FeS_2 microparticles, the value was 65% and 37%, respectively. In addition, due to the self-photolysis behaviour of MB caused by the visible light illumination, the degradation rate induced by the visible light was also investigated (Figure 4d), the degradation was about 2% within 2h and thus the degradation of MB itself under visible light could be ignored. It should be noted that the lower plateau degradation efficiency of the films (not reach to 100% degradation rate) compared with that of the pyrite or hematite powders could be ascribed to the photocatalysts loading capacity [27, 42], the dosage of the pyrite or hematite crystals in the films was lower than that of the powders, and the limitation of the dosage lead to the uncompleted degradation within short reaction periods [12,14]. Based on the degradation curves, the linear plot of $\ln(c/c_0)$ versus the reaction time could be regarded as the pseudo-first-order reaction, approximately as Figure 5 showed. And the function was $ln(c/c_0) = kt$.[43] c_0 is the initial concentration of the MB, the c is the concentration of MB after being illuminated for t min, k is the reaction rate constant. The reaction rate constant of FeS_2 nanotubes with 0.00902 min^{-1} demonstrated the advantages of pyrite nanotubes on the photodegradation compared with the other samples.

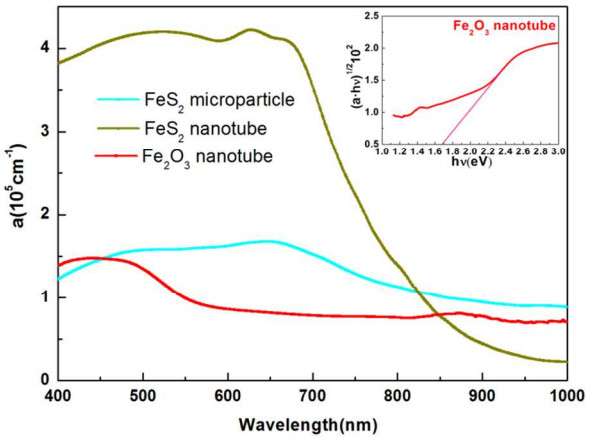

Fig. 3 Optical absorption property of different samples and the photo absorption coefficient of Fe_2O_3 nanotube array film

Figure 6 illustrated the degradation of phenol for various catalysts under the visible light illumination. Pyrite nanotubes coating significantly degraded phenol in 2.5h, the total reduction reached to approximately 60%. Compared with the pyrite nanotubes, pyrite piled microparticles coating degraded phenol slowly, and the decomposition only occupied below 40%. By contrast, the photocatalytic activity of hematite nanotubes in degradation of phenol was subtle, less than 10% of total phenol was reduced, which suggested that the mechanism of degradation of MB with of Fe_2O_3 nanotubes should be different from that of pyrite coatings.

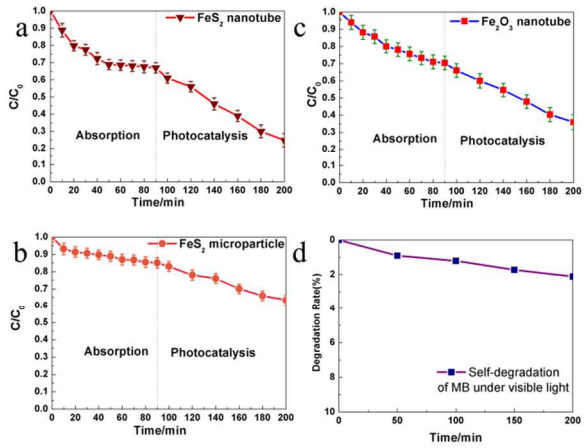

Fig. 4 Absorption and photocatalytic degradation ratios of MB for different coatings: (a) FeS_2 nanotubes, (b) Fe_2O_3 nanotubes and (c) FeS_2 piled microparticles; d) Self-degradation of the MB under the visible-light illumination

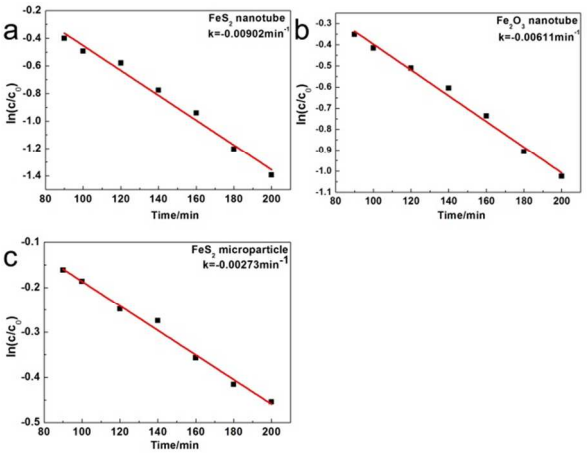

Fig. 5 Comparision of photocatalytic degradation rates of MB for nanotube films and microparticles films

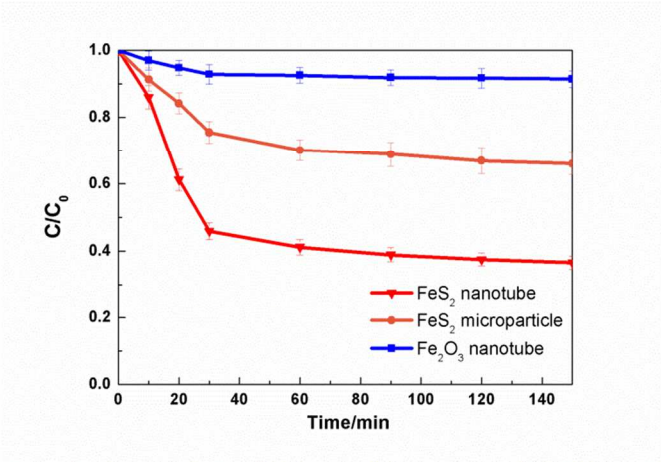

Fig. 6 Photodegradation curves of phenol for various catalysts

3.4 Mechanism of the degradation under the dark condition

Pyrite with the sufficient band gap (0.95eV) could generate photoinduced electron/hole pairs under the illumination of visible light (reactions 1-3).[30] The holes would react with the electron donor, such as water, and lead to the production of ·OH. In addition, in the aerobic aqueous environment the thermodynamic property of pyrite was unstable,[44] the molecular oxygen in the aqueous environment could lead to the oxidation of pyrite (reactions 4-6), and the oxidants such as ·OH and H_2O_2 might be generated during the oxidation process (reactions 7-13).[30, 45-47] The hydroxyl radicals generated by the photoactivation or the oxidation could result in the decomposition of organic pollutants and dyes. Here, the mechanisms of the degradation of MB would be elucidated under the dark and illumination, respectively.

Under the dark condition, the reduction of MB might be caused by the adsorption of the coatings and the oxidation of pyrite. Regarding to the adsorption, the adsorption rate was governed by the surface area.[14] In this study, the FeS_2 nanotubes film was fabricated through sulfidation of the precursor nanotubes film, and the sulfidation did not affect the morphology of the nanotubes (as Figure 1 showed), thus the surface area of Fe_2O_3 nanotubes might be approximate to the pyrite nanotubes. To investigate the surface areas between nanotubes and piled microparticles, the immersion test was employed. The concentration of K^+ follows the order nanotubes coatings < piled microparticles as Table S1 showed. Also it was noted that the values of the Fe_2O_3 nanotubes and FeS_2 nanotubes were close. The immersion test indicated that the nanotubes topography increased the surface area of the coatings compared with the piled microparticles, and might be advantage to the adsorption of dye.

$$FeS_2 + h\nu \rightarrow e^- + h^+ \quad (1)$$

$$h^+ + H_2O \rightarrow H^+ + \cdot OH \quad (2)$$

$$O_2 + e^- \rightarrow O_2^{\cdot -} \quad (3)$$

$$2FeS_2 + 7O_2 + 2H_2O \rightarrow 2Fe^{2+} + 4SO_4^{2-} + 4H^+ \quad (4)$$

$$FeS_2 + 14Fe^{3+} + 8H_2O \rightarrow 15Fe^{2+} + 2SO_4^{2-} + 16H^+ \quad (5)$$

$$2Fe^{2+} + 1/2\,O_2 + 2H^+ \rightarrow 2Fe^{3+} + H_2O \quad (6)$$

On the other hand, the behaviours of oxidation of pyrite might lead to the degradation of MB. Pyrite immersed in the solutions with pH below 3 would release iron ions, and the dissolved ferrous ions can react with O_2 to produce H_2O_2, which would result in the Fenton reactions (reaction 9).[48] However, with the pH ranging from acid to neutral, the reaction proceeding of ferrous release would be inhibited and replaced by the oxidation process gradually (reaction 10); in the neutral solution, the surface of pyrite would be decorated with Fe(III)-oxide patches, and the ferric ions was insoluble in near netural solutions.[49] In our study, the MB solutions under the dark were near neutral (as Table S1 showed), thus, instead of the Fenton

reaction caused by the dissolved ferrous ions, the oxidation of pyrite was the dominant reaction proceeding.

$$Fe^{II}_{aqueous} + O_2 \rightarrow Fe^{III}_{aqueous} + O_2^{\bullet -} \quad (7)$$

$$Fe^{II}_{aqueous} + O_2 + 2H^+ \rightarrow Fe^{III}_{aqueous} + H_2O_2 \quad (8)$$

$$Fe^{2+} + H_2O_2 \rightarrow Fe^{3+} + \bullet OH + OH^- \quad (9)$$

$$Fe^{II}_{pyrite} + O_2 \rightarrow Fe^{III}_{pyrite} + O_2^{\bullet -} \quad (10)$$

$$Fe^{II}_{pyrite} + O_2^{\bullet -} + 2H^+ \rightarrow Fe^{III}_{pyrite} + H_2O_2 \quad (11)$$

$$Fe^{III}_{pyrite} + H_2O \rightarrow Fe^{II}_{pyrite} + \bullet OH \quad (12)$$

$$2 \cdot OH \leftrightarrow H_2O_2 \quad (13)$$

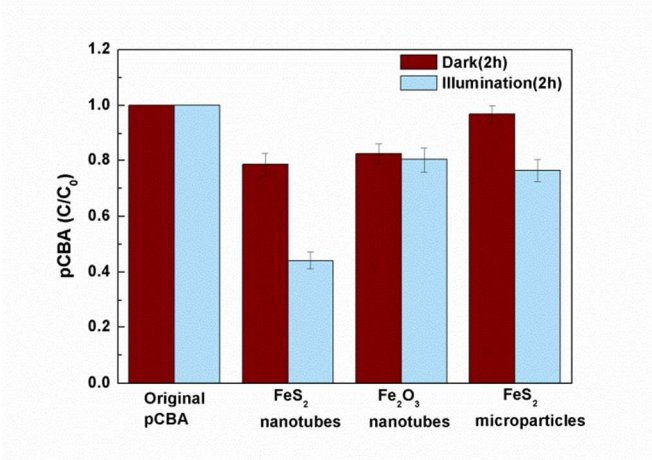

Fig. 7 The reduction of pCBA with various catalysts

To further verify the oxidation behaviour, measurements of iron and sulfate radicals concentrations in the solutions were employed. Regarding to the deviation caused by the iron release rate in the neutral solution, the test of sulfate radical concentration was used as the synergy. As Table S1 showed, little iron ions was detected, correspondingly, the concentration of the sulfate radicals was also below the detection line. In addition, the presence of the $Fe^{(III)}{\equiv}O$ peak after immersion further demonstrate the oxidation of $Fe^{(II)}$ (as Figure S1 showed). The formation of the $Fe^{(III)}$ oxide might lead to the generation of the hydroxyl radicals and hydroxyl peroxide (reactions 11 and 12). Specially, ·OH can combine to form H_2O_2 (reaction 13), and the production of ·OH would be inhibited in the neutral solution.[30] Therefore, H_2O_2 should be the main product in the MB solutions immersed with the pyrite coatings in the dark. In regard to the activity of Fe_2O_3, the previous studies have demonstrated that the Fe_2O_3 was an inactive catalyst and stable in neutral solution, even though introducing H_2O_2,[41] and the iron ions concentration illustrated in table S1 also confirmed the insolubilization of the Fe_2O_3 nanotubes, correspondingly. Para-chlorobenzoic acid (pCBA) was always used to detect the ·OH in aqueous environment.[50] To further verify the oxidants in the MB solution, the reduction of pCBA by various catalysts were measured as Figure 7 showed. Because of the inactivation, the reduction of pCBA by the Fe_2O_3 nanotubes coating could be attributed to the adsorption. Therefore, compared with the Fe_2O_3 nanotubes, the approximate or the less reduction indicated the negligible production of hydroxyl radicals generated by the pyrite coatings. In addition, H_2O_2 hardly had any catalytical reactivity as Figure S2 showed. Thus, although the pyrite coatings could produce oxidants under the dark condition, regardless of the topography, the contribution to the decomposition of MB was subtle and the reduction of MB should be attributed to the adsorption. Based on the above elucidation, the nanotubes coatings with higher surface area could enhance the reduction of MB under the dark condition.

3.5 Mechanism of the degradation under illumination

Under the visible light irradiation, the photoexcited pyrite would generate the hydroxyl radicals which could mineralize MB. However, in consideration of the influence of hydroxyl radicals on the oxidation of pyrite, here, we would first investigate the oxidation behavior of pyrite coatings irradiated by the visible light.

Previous studies have demonstrated that in the neutral solution, the oxidation of pyrite under visible light illumination was strongly dependent on the temperature.[44] The visible light induced thermal effect would lead to the higher temperature, which could promote the oxidation rate of pyrite. However, the photocatalytic experiments were performed in the constant temperature in our study, and the MB solution was near neutral during the whole photodegradation as Figure S3 a-c showed. Therefore, the light induced heat could be ignored. In this study, according to the data in Table S1, the change of iron release and sulfate radical in the solution after illumination was subtle, which suggested the visible light illumination contributed to the oxidation and the dissolution of pyrite slightly. In addition, it is also noted that the $Fe^{III}_{(hematite)}$ of the Fe_2O_3 nanotubes irradiated by sunlight was also insoluble as Table S1 showed.

Because the effect of illumination on the oxidation of pyrite was negligible, the degradation of MB should be attributed to the photocatalysis or the dye photosensitization.[51,52] Although the pyrite and hematite can produce the hydroxyl radical irradiated by visible light, the intrinsic mid-band gap states and trap-states might promote the recombination of hole and electron, which could deactivate the photocatalysis.[41,53] Therefore, the production of photoinduced ·OH was measured via reducing the concentration of pCBA to evaluate the photoactivities of pyrite and hematite coatings. As Figure 7 showed, pyrite coatings with nanotubes or piled microparticles structure can reduce the concentration of pCBA significantly. Especially, after treated with pyrite nanotubes for 2h, the pCBA was reduced by 42%. However, Fe_2O_3 nanotubes can hardly reduce the concentration of pCBA, which indicated that the decomposition of MB caused by the hematite nanotubes might be attributed to the dye self-sensitized process (reactions 14,15). For avoiding the dye photosensitization, phenol as a photostable organic pollutant was employed to investigate the mechanism of the photocatalysis. As Figure 6 showed, the degradation of phenol with of Fe_2O_3 nanotubes could be

negligible; on the contrary, the pyrite nanotubes and microparticles coatings lead to a significant reduction of phenol under the visible light illumination, respectively.

$$Dye + h\nu \rightarrow dye^{*} \quad (14)$$

$$Dye^{*} + Fe_2O_3 \rightarrow dye^{+\bullet} + e^{-}_{cb} \quad (15)$$

Respecting to the slight degradations of phenol and pCBA, it should be concluded that with the irradiation of visible light, Fe_2O_3 nanotubes was inactive compared with the pyrite nanotubes or piled microparticles. Actually, the unsatisfactory photocatalytic capacity of Fe_2O_3 has been recognized.[54] In addition, previous studies have demonstrated the solar light driven photocatalytic activity in the degradation of MB and phenol. Compared with MB, phenol was reduced negligibly.[53] Further, the mid-band gap of Fe_2O_3 nanotubes and the photoinduced electrons transfer (ET) from excited dye to Fe_2O_3 would be investigated in our future study.

Based on the photocatalytic behaviour discussed above, it is reasonable to conclude that the photoactivities of pyrite coatings in degrading dye and organic pollutant should be mainly ascribed to the generation of ·OH. However, it is also interesting to note that regardless of MB and phenol, the photocatalytic capacity of pyrite nanotubes coating was enhanced compared with the piled microparticles coating. Because of the higher surface area, pyrite nanotube coatings could generate more photoinduced holes at the interface of solutions/solid films, promote light harvesting, [15,35] and improve the photoelectrochemical properties.[55-57] Specially, the higher surface area also could accelerate the adsorption of dye molecules on the photocatalyst,[42] thus, compared with the pyrite piled microparticles coating, the hematite nanotubes increased the photodegradation rate of MB. However, the wider indirect band gap of hematite with 1.69eV might attenuate the performance of the light harvesting,[58] and resulted in the poor photoinduced hydrophilic (as Figure S3 d showed),[12] eventually lead to the decreased degradation rate compared with the pyrite coatings with the similar nanotubes structure. Besides the higher surface area, retarding the recombination of the photoinduced electron/hole pairs would improve the photocatalysis.[59] The space charge layer within the nanotube walls would inhibit the recombination of the hole/electron pairs and promote the separation behaviour. [14,60] Therefore, pyrite nanotubes coating could enhance the adsorption of dye and the separation of the e^{-}/$hole^{+}$ pairs, which contributed to the decomposition of MB and phenol.

In addition, although the photodegradation of MB with of pyrite coatings should be mainly ascribed to the photocatalysis, the dye self-sensitization might influence the degradation process. Therefore, the interplay between the photoexcited dye molecule and the pyrite should be investigated in our future studies.

4. Conclusions

The stoichiometric ratio FeS_2 nanotubes displayed excellent photocatalysis behaviour on degradation of MB and phenol in solutions, respectively. The distinction between the degradation of MB and phenol for Fe_2O_3 nanotubes might be attributed to the dye photosensitization. Although the dissolved ferrous ions in this study were negligible, to use the pyrite nanotubes in the Fenton system is a considerable strategy in water treatment. The Fenton-pyrite nanotube system for water treatment and the photosensitization of MB will be investigated in our future studies.

Acknowledgements

We thank the National Natural Science Foundation of China (U1261120), Post-Doctoral Foundation of China (2013M530930), Scientific Foundation of Educational Department of Liaoning Province (L2012084), Project of Ministry of Education of Basic Scientific Research (N130402001). Science Foundation of China University of Petroleum Beijing (No. 2462014YJRC011), Open fund from State Key Laboratory of Metal Matrix Composites, Shanghai Jiaotong University (mmckf-14-11) for the support.

Notes and references

[a]Institute of Metallurgical Resources and Environmental Engineering, Northeastern University, Shenyang 110819, China. Email: Tiana@smm.neu.edu.cn (Ang Tian), Xuexx@smm.neu.edu.cn (Xiangxin Xue)

[b] Institute of New Energy, State Key Laboratory of Heavy Oil Processing, China University of Petroleum, Beijing 102249, China.

[c]School of Materials Science and Engineering, Shenyang University of Technology, 111 Shenliao West Road, Economic & Technological Development Zone, 110178 Shenyang, China.

[d]School of Resources and Materials, Northeastern University at Qinhuangdao Branch, Qinhuangdao, 066004, P. R. China.

[e]Department of Civil and Environmental Engineering, Rice University, Houston, Texas 77005, United States.

• The authors contributed equally to this work

1 K. Zhang, X.F. Du, M.B. Katz, B.H. Li, S.J. Kim, K.X. Song, G.W. Graham, X.Q. Pan, *Chem Commun*, 2015, **51**, 8584

2 Q. Xu, J. Zhao, Y. Liu, P. Pu, X. Wang, Y. Chen, C. Gao, J. Chen, H. Zhou, *J Mater Sci*, 2015, **50**, 2571-2576.

3 Q. Xu, P. Pu, J. Zhao, C. Dong, C. Gao, Y. Chen, J. Chen, Y. Liu, H. Zhou, *J Mater Chem A*, 2015, **3**, 542

4 P.V. Kamat. *J Phys Chem Lett*, 2012, **3**, 663.

5 M. Kapilashrami, Y.F. Zhang, Y.S. Liu, A. Hagfeldt, J. Guo. *Chem Rev*, 2014, **114**, 9662.

6 I. Cesar, A. Kay, J.A. Gonzalez-Martinez, M. Grazel, *J. Am. Chem. Soc.*, 2006, **128**, 4582.

7 X. Chen, S.S. Mao, *Chem Rev*, 2007, **107**, 2891.

8 W.X. Zhang, Z. Yang, X. Wang, Y.C. Zhang, X.G. Wen, S.H. Yang, *Catal Commun*, 2006, **7**, 408.

9 B.D. Alexander, P.J. kulesza, L. Rutkowska, R. Solarska, J. Augustynski, *J Mater Chem*, 2008, **18**, 2298.

10 C.K. Gu, C. Shannon, *J Mol Catal A-Chem*, 2007, **262**, 185.

11 Z.Y. Liu, X.T. Zhang, S. Nishimoto, T. Murakami, A. Fujishima, *Environ Sci Technol*, 2008, **42**, 8547

12 Q. Li, J.K. Shang, *Environ Sci Technol*, 2010, **44**, 3493.
13 D.N.Tafen, R. Long, O.V. Prezhdo, *Nano Lett*, 2014, **14**, 1790.
14 H.F. Zhuang, C.J. Lin, Y.K. Lai, L. Sun, J. Li, *Environ Sci Technol*, 2007, **41**, 4735.
15 Y. Hou, X. Li, X. Zou, X. Quan, G. Chen, *Environ Sci Technol*, 2009, **43**, 858.
16 H. Zhou, J.Y. Pan, L. Ding, Y.W. Tang, J. Ding, Q.X. Guo, T.X. Fan, D. Zhang, *Int J Hydrogen Energ*, 2014, **39**, 16293.
17 A. Ennaoui, S, Fiechter, C. Pettenkofer, N. Alonso-Vante, K. Büker, M. Bronold, C. Höpfner, H. Tributsch, *Sol Energ Mat Sol C*, 1993, **29**, 289.
18 K. Sun, Z. Su, J. Yang, Z. Han, F. Liu, Y. Lai, J. Li, Y. Liu, *Thin Solid Films*, 2013, **542**, 123.
19 X. Qiu, M. Liu, T. Hayashi, M. Miyauchi and K. Hashimoto, *Chem. Commun.*, 2013, **49**, 1232.
20 Y. Bi, Y. Yuan, C. Exstrom, S. Darveau, J. Huang, *Nano Lett.*, 2011, **11**, 4953.
21 S. Shukla, N.H. Loc, P.P. Boix, T.M. Koh, R.R. Prabhakar, H. Mulmudi, J. Zhang, S. Chen, C.F. Ng, C.H.A. Huan, N. Mathews, T. Sritharan, Q. Xiong, *ACS Nano*, 2014, **8**, 10597.
22 D. Liang, M. Cabán-Acevedo, N. S. Kaiser, S. Jin, *Nano. Lett*, 2014, **14**, 6754
23 K. Büker, N. Alonso-Vante, H. Tributsch, *J. Appl. Phys.*, 1992, **72**, 5721.
24 M. Cabán-Acevedo, D. Liang, K.S. Chew, J.P. DeGrave, N.S. Kaiser , S. Jin, *ACS Nano*, 2013, **7**, 1731.
25 J. Jiao, L. Chen, D. Kuang, W. Gao, H. Feng, J. Xia, *RSC Adv*, 2011, **1**, 255.
26 S. Middya, A. Layek, A. Dey, P. P. Ray, *J. Mater. Sci. Technol.*, 2014, **30**, 770.
27 S. Liu, M. Li, S. Li, H. Li, L. Yan, *Appl Surf Sci*, 2013, **268**, 213
28 K. Choi, S. Bae, W. Lee, *J Hazard Mater*, 2014, **280**, 31.
29 S. Bae, D. Kim, W. Lee, *Appl Catal B-Environ*, 2013, **134**, 93.
30 L.H. Kong, X.Y. Hu, M.C. He, *Environ Sci Technol*, 2015, **49**, 3499.
31 Y.Y. Song, Z.D. Gao, P. Schmuki, *Electrochem Commun*, 2011, **13, 290**
32 M.D. Wang, C.C. Xing, K. Cao, L. Zhang, J.B. Liu, L. Meng, *J. Mater. Chem. A*, 2014, **2**, 9496
33 H.A. Macpherson, C.R. Stoldt, *ACS Nano*, 2012, **6**, 8940.
34 W. Li, M. Doblinger, A. Vaneski, A. L. Rogach, F. Jackel, J. Feldmann, *J. Mater. Chem.*, 2011, **21**, 17946.
35 X. Shi, A. Tian, X.X. Xue, H. Yang, Q. Xu, *Mater. Lett*, 2015, **141**, 104.
36 R. Morrish, R. Silverstein and C.A. Wolden, *J. Am. Chem. Soc.*, 2012, **134**, 17854.
37 B. Yuan, W. Luan, S. Tu, *Dalton T.*, 2012, **41**, 772.
38 M.Y.C. Teo, S.A. Kulinich, O.A. Plaksin, A.L. Zhu, *J. Phys. Chem. A.*, 2010, **114**, 4173.
39 Y. Bai, J. Yeom, M. Yang, S.H. Cha, K. Sun, N.A. Kotov, *J. Phys. Chem. C*, 2013, **117**, 2567.
40 D. Susac, L. Zhu, M. Teo, A. Sode, K.C. Wong, P.X. Wong, R.R. Parsons, D. Bizzotto, K.A.R Mitchell and S.A. Campbell, *J. Phys. Chem. C*, 2007, **111**, 18715.
41 L. Guo, F. Chen, X. Fan, W. Cai, J. Zhang, *Appl Catal B-Environ*, 2010, **96**, 162.
42 G.Y. Zhang, Y. Feng, Y.Y. Xu, Dong-Zhao Gao, Y.Q. Sun, *Mater Res Bull*, 2012, **47**, 625.
43 X.M. Song, J.M. Wu, L. Meng, M. Yan, *J. Am. Ceram. Soc.*, 2010, **93**, 2068.
44 M. Schoonen, A. Elsetinow, M. Borda, D. Strongin, *Geochem. T.*, 2000, **1**, 23.
45 C.A. Cohn, S. Mueller, E. Wimmer, N. Leifer, S. Greenbaum, D.R. Strongin, M.A.A. Schoonen, *Geochem. T.*, 2006, **7.**
46 D.W. King, *Environ. Sci. Technol.*, 1998, **32**, 2997.
47 J.D. Rush, B.H.J. Bielski, *J. Phys. Chem.*, 1985, **89**, 5062
48 B. Tryba, A.W. Morawski, M. Inagaki, M. Toyoda, *Appl Catal B-Environ*, 2006, **63**, 215.
49 C.M. Eggleston, J.J. Ehrhardt, W. Stumm, *Am. Mineral.*, 1996, **81,** 1036.
50 L. Brunet, D.Y. Lyon, E.M. Hotze, P.J.J. Alvarez, M.R. Wiesner, *Environ. Sci. Technol.*, 2009, **43**, 4355.
51 L. Pan, J.J. Zou, X.W. Zhang, L. Wang, *J. Am. Chem. Soc.*, 2011, **133**, 10000
52 X.L. Yan, T. Ohno, K. Nishijim, R. Abe, B. Ohtani, *Chem Phys Lett.,* 2006, 429, 606-610.
53 G.K. Pradhan, K.M. Parida, *ACS Appl. Mater. Interfaces.,* 2011, **3**, 317
54 R. Matta, K. Hanna, S. Chiron, *Sci. Tot. Environ.,* 2007, **385**, 242.
55 G.K. Mor, O.K. Varghese, M. Paulose, K. Shankar, C.A. Grimes, *Sol. Energ. Mater. Sol. C*, 2006, **90**, 2011.
56 K. Zhu, N.R. Neale, A. Miedaner, A.J. Frank, *Nano Lett,* 2007, **7**, 69
57 I.S. Cho, Z. Chen, A.J. Forman, D.R. Kim, P.M. Rao, T.F. Aramillo, X. Zheng, *Nano Lett.*, 2011, **11**, 4978.
58 A.A. Akl, *Appl Surf Sci*, 2004, **233**, 307.
59 H. Chen, S. Chen, X. Quan, H, Yu, H. Zhao, Y. Zhang, *J. Phys. Chem. C*, 2008, **112**, 9285.
60 R. Beranek, H. Tsuchiya, T. Sugichima, J.M. Macak, L. Taveira, S.Fujimoto, H. Kisch, P. Schmuki, *Appl. Phys. Lett.*, 2005, **87**, 243114.

Graphical Abstract

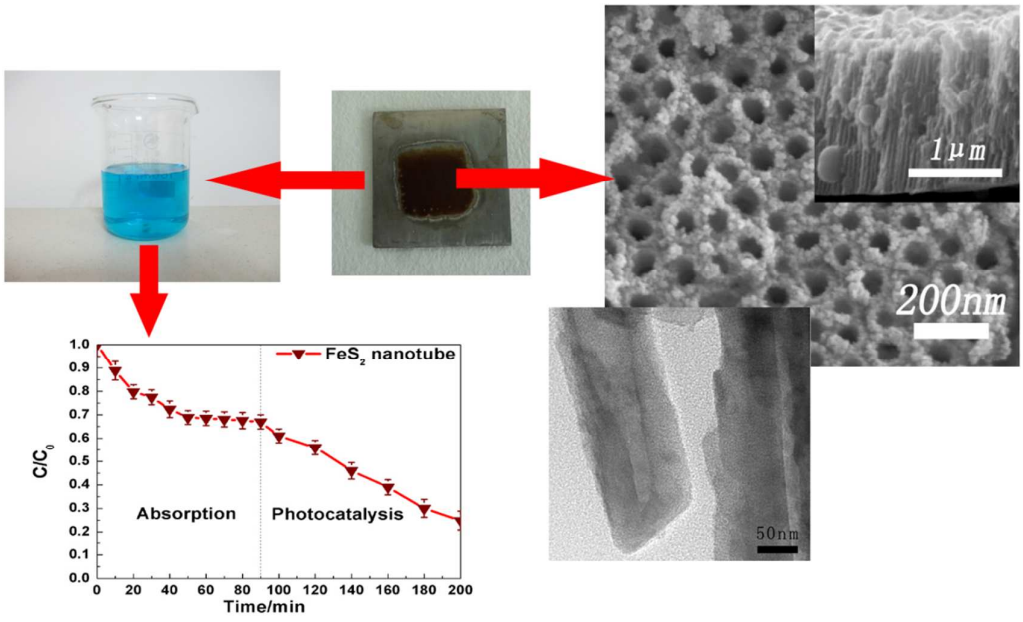

The nanotube topography would improve the optical property of the pyrite crystals. The photodegradation of MB and phenol suggested that the pyrite nanotubes array films would be potential to be used in the treatment of pollutants.